2001

Comparison of the Monthly Precipitation Derived from the TRMM Satellite

D. Shin
George Mason University

L. Chiu
Taipei City Hosp

Menas Kafatos
Chapman University, kafatos@chapman.edu

Recommended Citation
Shin, D., Chiu, L.S., Kafatos, M. (2001). Comparison of the Monthly Precipitation Derived from the TRMM Satellite, *Geophysical Research Letters*, Vol. 28, No. 5, 795-798. doi: 10.1029/2000GL012162

Comparison of the Monthly Precipitation Derived from the TRMM Satellite

GEOPHYSICAL RESEARCH LETTERS, VOL. 28, NO. 5, PAGES 795-798, MARCH 1, 2001

Comparison of the Monthly Precipitation Derived from the TRMM Satellite

Dong-Bin Shin, Long S. Chiu and Menas Kafatos

Center for Earth Observing and Space Research, George Mason University, Fairfax, Virginia

Abstract. A comparison of monthly rainfall derived from the version 5 of TRMM Microwave Imager (TMI), Precipitation Radar (PR), TRMM Combined algorithm (TCA) and TMI-emission algorithm (TMIE) using two years (1998 to 1999) of TRMM data was made. The global (TRMM domain, 40°N~ 40°S) average rain rates are 3.29, 2.62 and 2.93 mm/day over land and 3.02, 2.47 and 2.54 mm/day over oceans for TMI, PR, and TCA respectively. The TMIE oceanic average is 2.90 mm/day. For both the global and zonal means, the TMI rain rates are the largest and the PR estimates lowest. Regression analyses show the offsets of algorithms are close to zero. According to a paired t-test, significant differences exist between TMI and PR and between TMI and TCA, especially in oceanic dry regions. However, the difference between PR and TCA was judged to be insignificant. Comparison of PR and TMIE shows that a statistically significant difference is evident in the oceanic dry regions.

Introduction

Precipitation is a major component of the global energy and hydrological cycle and hence affects the global climate in many ways. The latent heat release associated with the precipitation process is a major driving force for atmospheric circulations. The variability of tropical precipitation affects weather changes worldwide and the livelihood of a large fraction of the world population [*Simpson*, 1992]. Precipitation influences the vegetation cover, which in turn modifies the radiation balance. Precipitation induced fresh water flux changes the oceans' surface salinity, thereby the stability of the ocean column, air-sea exchanges and water mass formation [*Hartmann*, 1994]. Accurate measurements of tropical precipitation are therefore crucial for advancing our understanding of the variability of the climate system and improving climate predictions.

A series of microwave sensors have been developed to measure global precipitation, beginning with the deployment of the Electrically Scanning Microwave Imager on board the Nimbus-5 satellite in 1972. More recently, the Tropical Rainfall Measuring Mission (TRMM) satellite was launched in November 1997 [*Simpson et al.*, 1988] with an inclination of approximately 35° and an altitude of 350 km. TRMM was designed to address some important errors in microwave retrievals such as the beam-filling errors [*Chiu et al.*, 1990] and the diurnal bias [*Shin and North*, 2000]. There are five instruments on board the TRMM satellite, three of which are part of the TRMM rainfall package: Microwave Imager (TMI), the first space-borne Precipitation Radar (PR), and a Visible Infrared Scanner [*Kummerow et al.*, 1998].

One of the objectives of TRMM is to produce a multi-year time series of monthly rainfall with a resolution of $5° \times 5°$ latitude-longitude with an accuracy of 1 mm/day or 10% in heavy precipitation at that scale. It is therefore important first to understand the biases between TRMM rain algorithms. In this study, we investigate the performance of four standard TRMM algorithms: TMI profiling (or 2A12 as referenced by the TRMM Science Data and Information System, TSDIS), PR rain profile (2A25), TRMM Combined PR/TMI rain rate (2B31, hereafter TCA) and monthly rainfall from TMI-emission algorithm (3A11, hereafter TMIE).

TRMM rainfall data

Following the SSM/I heritage, the TMI measures microwave radiances emitted by the Earth and atmosphere from nine channels at five frequencies (10.7, 19.4, 21.3, 37.0 and 85.5 GHz). An additional channel at 10.7 GHz provides a better dynamic range for detecting heavy rainfalls that are prevalent in the tropics. The TMI profiling algorithm (2A12) over oceans employs multi-dimensional cloud models to construct a database of hydrometeor profiles and their computed brightness temperatures. Using a Baysian approach, the TMI rainfall is derived from the observed brightness temperatures [*Kummerow et al.*, 1996]. Over land, rain rates are calibrated against the high frequency channels.

The TMIE algorithm uses a simple cloud model and a plane-parallel radiative transfer model to find the relationship between the upwelling microwave radiance and rain rate. The rain rates are assumed to follow a mixed-lognormal distribution. The parameters of the rain rate distribution is computed by matching the histogram of brightness temperature [*Wilheit et al.*, 1991].

The PR operates at 13.8 GHz and measures the return power with a vertical spacing of 250 m for nor-

Paper number 2000GL012162.
0094-8276/01/2000GL012162$05.00

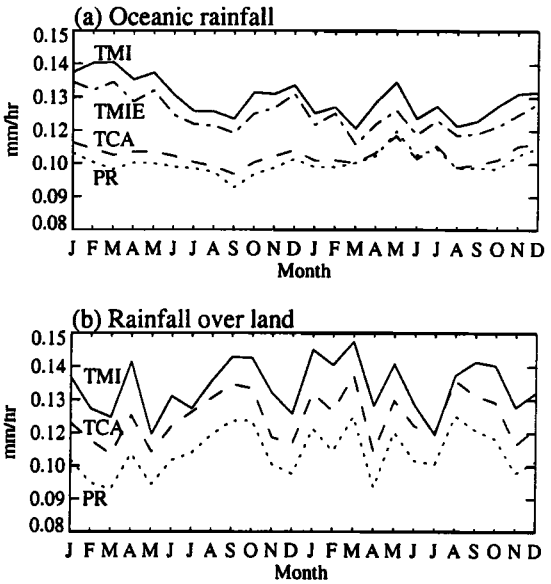

Figure 1. Monthly global mean rain rate for each algorithm from the $5^o \times 5^o$ longitude-latitude grid data over ocean (a) and land (b).

mal samples. The PR has a swath width of 215 km and completes a scan every 0.6 s. The PR rainfall algorithm (2A25) estimates rain profile using the relationship between attenuation-corrected radar reflectivity and rain rate. The details of the PR algorithm are given by *Iguchi and Meneghini* [1994]. The TCA algorithm (2B31) computes rain rates by estimating drop size distributions of hydrometeors derived from the PR reflectivities and TMI attenuation measurements [*Haddad et al.*, 1997].

We binned the surface rain data from the TMI, PR and TCA algorithms in $0.5^o \times 0.5^o$ and $5^o \times 5^o$ longitude-latitude grid boxes and compute monthly rain rates based on the gridded data. The TMIE data are provided by the algorithm developer who noted a coding error in the version 5 TMIE algorithm that was submitted to TSDIS (A. T. C. Chang, private communication, 2000). We used the corrected version of the TMIE data.

Comparison of the monthly rain data

Global means

The global average rain rates computed from the $5^o \times 5^o$ longitude-latitude grid data over the two-year period are 3.1, 2.52 and 2.64 mm/day for TMI, PR and TCA, respectively, while the TMIE shows an oceanic average of 2.9 mm/day. The root-mean squared differences are 1.72 mm/day between TMI and PR, 0.61 mm/day between PR and TCA and 1.07 mm/day between TMI and TMIE. Figure 1 shows the time series of monthly global mean rain rates over ocean and land calculated from the gridded data. For the global ocean mean (1a) the algorithms tend to cluster into two groups, i.e., the TMI and TMIE show larger estimates than PR and TCA. Generally, the differences between algorithms over ocean are larger during 1998, especially for the first half of 1998, than 1999. The larger difference (more than 10% from the mean of all the algorithms) may be related to uncertainty in measurements of precipitation having a high variability associated with the 1998 El Niño episode. The algorithm difference in global average rain rates are larger over land than over ocean (1b). Furthermore, the difference does not seem to correlate with the seasons. The large difference may be due to the highly variable rainfall patterns over land and the different TMI algorithms used over land and ocean. The TMI estimate is the largest for all seasons while the PR the lowest. The global mean of TCA is close to the mean of all three algorithms.

We investigated the distribution of the algorithm that estimates the largest two-year mean rain rate over $0.5^o \times 0.5^o$ and $5^o \times 5^o$ longitude-latitude grid boxes. In general, the TMI estimates are highest over the heavy rain, such as the inter-tropical convergence zone (ITCZ), while the PR and TCA are higher at lower rain regions. For oceanic rain, the TMIE rain rate turns out to be the highest in the oceanic dry regions.

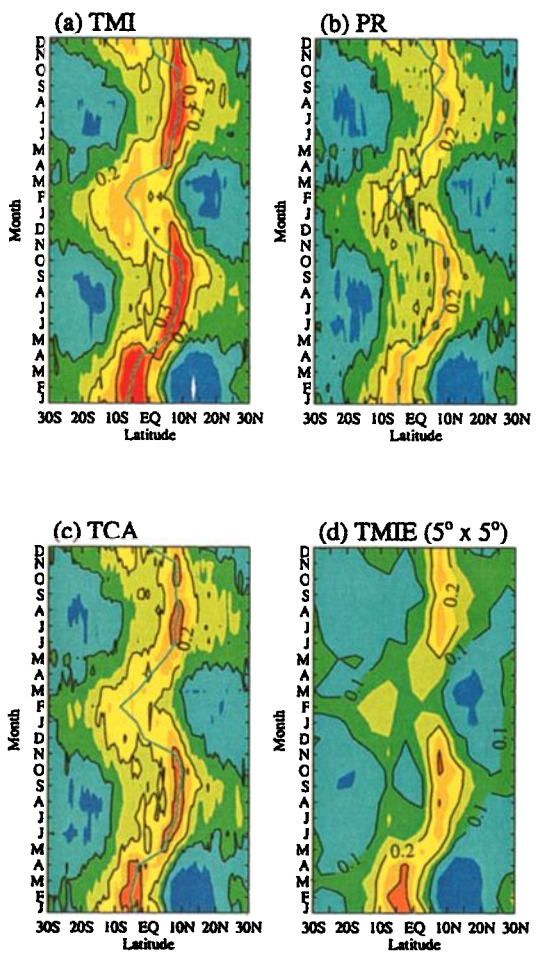

Figure 2. Time-latitude diagram of the zonal mean rain rates. Contour interval is 0.05 mm/hr and every 1.0 mm/hr is indicated by solid line. The superimposed (cyan) line in the first three panels represents the monthly mean location of the ITCZ.

Zonal means

Time-latitude diagram of zonally averaged monthly rain rate is shown in Fig. 2 using the $0.5^o \times 0.5^o$ longitude-latitude grid data for TMI, PR and TCA and the $5^o \times 5^o$ grid data for TMIE. All algorithms show a strong seasonal cycle, especially in the ITCZ region. The extent of the region is greater for the TMI than the PR data suggesting that the TMI estimates larger precipitation rates than the PR or TCA. We also note that the convective zone in the Southern summer during the 1998 El Niño is more prominent than in 1999. The monthly mean location (latitude) of the ITCZ is also indicated in cyan. This is estimated from the following equation suggested by *Waliser and Gautier* [1993],

$$\overline{y} = \frac{\int R(y) y \, dy}{\int R(y) \, dy} \tag{1}$$

where y denotes the latitude in degrees and $R(y)$ represents the zonal mean rain rate at the latitude y. The integrals run from 20°S to 20°N. The estimated position of the ITCZ follows the high precipitation region except for periods with a double ITCZ, such as in November and December of 1999. All estimates have a very similar migration pattern. The migration of the high precipitation zone seems to show hemispheric asymmetry, with preference for the Northern Hemisphere. During the Northern summer, the ITCZ migrates farther toward the pole and stays longer than during the Southern summer. This hemispheric asymmetry of the ITCZ, as pointed out by some investigators, may be attributed to the difference of baroclinity between the hemispheres resulting from the large landmass and warmer sea surface temperature in the tropic of the Northern Hemisphere.

Regression analyses

Scatter diagrams of the $5^o \times 5^o$ longitude-latitude grid data for ocean and land are shown in Fig. 3. Regression analyses between TMI and PR from ocean data showed a slope of 0.69, an intercept of 0.02, and a correlation of 0.91 (3a). The regression line crosses the 1-1 line at 0.05. Very similar results (3b) are obtained for land data. Therefore, the PR rain rates are larger below 0.05 or 0.06 mm/hr, whereas the TMI rain rates are larger above the cross points. This is consistent with the distribution of the dominant algorithm discussed in the previous section. Regression analyses between PR and TCA (3c,d) show that these two estimates are highly correlated over both ocean and land. The slopes of the regression are 1.0 and 0.99 over ocean and land, respectively. A comparison between the TMI and TMIE oceanic rain rates is shown in the last panel (3e). The global mean of TMIE rain rate is smaller than the TMI rain rate by about 4% and the overall correlation is 0.96.

Paired t-test

We investigated the regional differences between the algorithms. The significance of the difference between two algorithms are tested using a paired t-test [*Chang et al.*, 1999]. The t statistic for the paired rain rates are defined as:

$$t = \frac{\overline{x} - \overline{y}}{\sigma_{xy}/N^{1/2}} \tag{2}$$

where $\overline{x}$ and $\overline{y}$ are the ensemble averages of the monthly mean data from two different algorithms, σ_{xy} is the standard deviation of $x - y$ and N is the number of pairs.

Figure 4 shows distribution of the t-statistic. For a two-tailed t-test using the 24 pairs of the monthly mean rain rates, $|t|$-values larger than 2.1 are significant at the 95% level and the null hypothesis that the two means are equal is rejected at the $p = 0.05$ level of significance. From the figure, the pairs of TMI/PR (4a) and TMI/TCA (4b), the areas with significant difference (TMI larger) seem to be located in the high rain regions. However, significant negative t values (PR or TCA larger) are found over some of the oceanic dry regions such as the southeastern Pacific. The t values between PR and TCA are small and statistically insignifi-

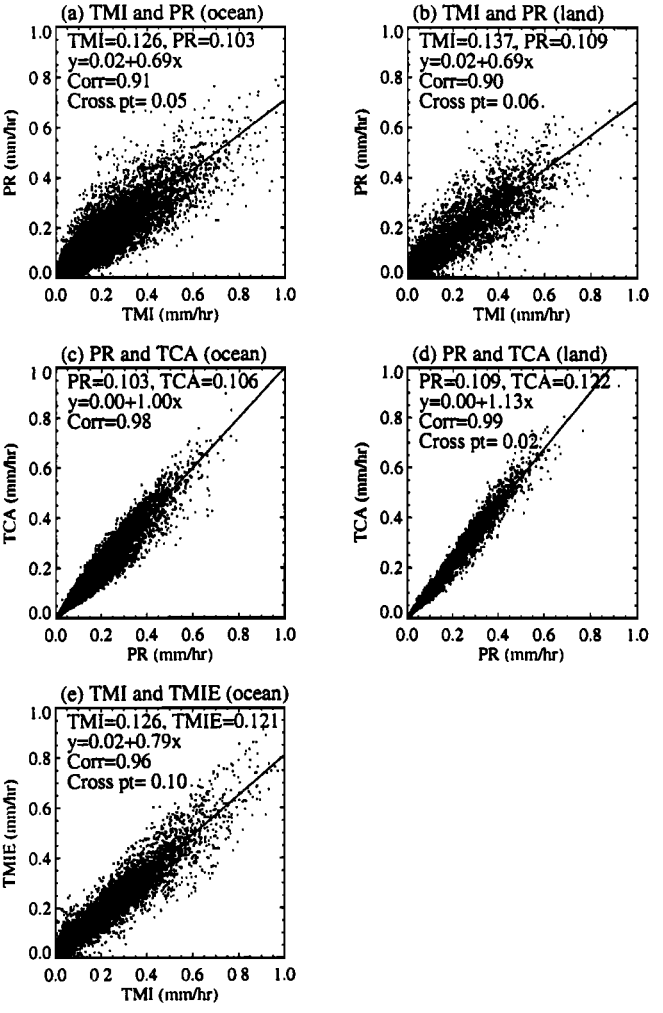

Figure 3. Scatter diagrams of the monthly mean data over $5^o \times 5^o$ longitude-latitude grid boxes for the period of two years. The regression line is indicated by solid line.

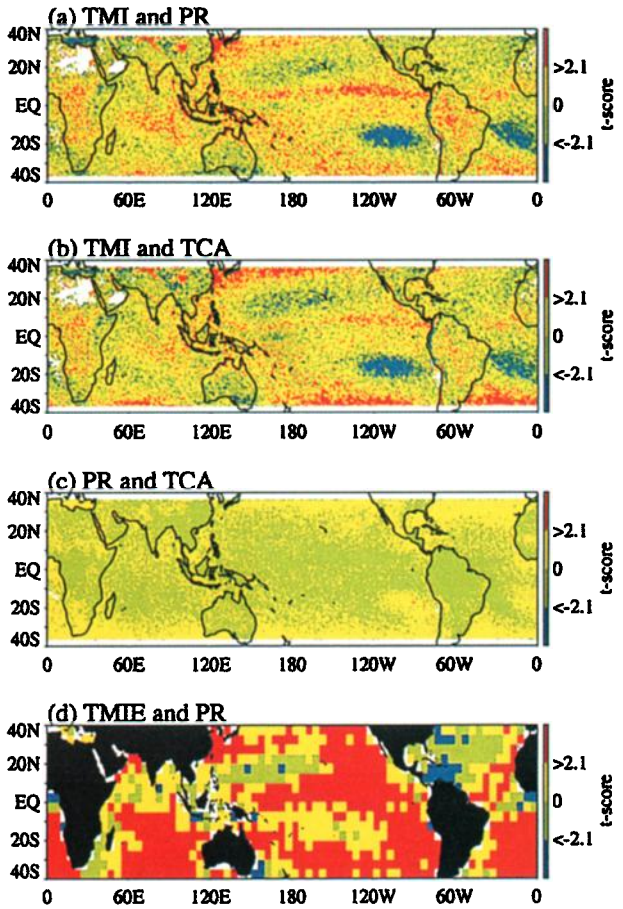

Figure 4. Distribution of t-statistic from a paired t-test.

cant. The TMIE tends to show significantly higher rain rates than PR in most regions.

Conclusions

We have examined the differences between the monthly rainfalls derived from the TRMM version 5 algorithms for the period from 1998 to 1999. The global-oceanic means from the TMI and TMIE are larger than those from the PR and TCA. The global-oceanic means of the algorithms vary within 10% of the algorithm average, except for the TMI and PR during the first half of 1998. During this period, the atmosphere experienced the strong 1997-1998 El Niño episode which is characterized by great variability in precipitation pattern. On the other hand, the global averages over land exhibit large fluctuations that illustrates the difficulty of the retrievals of land precipitation. Zonal mean analyses reveal that the rainfall products for all the algorithms exhibit similar seasonal variations, including migration of the ITCZ associated with precipitation maximum and the location of the dry area in the subtropics. The zonal mean of the TMI rainfall is the largest among all algorithms. Using a paired t-test, we found no significant difference between the PR and TCA rainfalls, whereas the TMI, PR and TCA rainfalls show significant difference in areas of extreme rainfall, such as the ITCZ and oceanic dry regions.

While all algorithms demonstrate similar temporal and spatial patterns, the rainfall intensities are quite different, probably due to details of algorithms and sampling characteristics. In future work, we will investigate other rain parameters such as rain fraction, conditional rain rate, rain-column height, stratiform and convective precipitation discrimination and the diurnal biases to better understand the behaviors of the TRMM algorithms. This knowledge will aid in the use of TRMM to calibrate historical rainfall estimates such as those derived from SSM/I and the Global Precipitation Climatology Project [*Chang et al.*, 1999].

Acknowledgments. We thank Dr. A. T. C. Chang for providing the corrected version 5 of TMIE data. The data used in this study are provided by the TRMM Science Data Information System (TSDIS) and the Goddard Earth Sciences Distributed Active Archive Center (GDAAC). This work is partially supported by NASA CAN NCC5-306. LSC is supported by NASA grant NAG5-9035.

References

Chang, A. T. C., L. S. Chiu, C. Kummerow and J. Meng, First results of the TRMM microwave imager (TMI) monthly oceanic rain rate: Comparison with SSM/I, *Geophys. Res. Lett., 26,* 2379-2382, 1999.

Chiu, L. S., G. R. North, A. McConnell, and D. A. Short, Rain estimation from satellites: Effect of finite field of view, *J. Geophys. Res., 95,* 2177-2186, 1990.

Haddad, Z. S., E. A. Smith, C. Kummerow, T. Iguchi, M. R. Farrar, S. L. Durden, M. Alves, and W. S. Olson, The TRMM 'Day-1' radar/radiometer combined rain-profiling algorithm, *J. Meteor. Soc. Japan, 75,* 799-809, 1997.

Hartmann, D. L. *Global Physical Climatology,* 409 pp., Academic, San Diego, Calif., 1994.

Iguchi, T., and R. Meneghini, Intercomparison of single frequency methods for retrieving a vertical rain profile from airborne or spaceborne data, *J. Atmos. Oceanic Tech., 11,* 1507-1516, 1994.

Kummerow, C., W. S. Olsen, and L. Giglio, A simplified scheme for obtaining prediction and vertical hydrometeor profiles from passive microwave sensors, *IEEE Trans. Geosci. Electron., 34,* 1213-1232, 1996.

Kummerow, C., W. Barnes, T. Kozu, J. Shiue, and J. Simpson, The tropical rainfall measuring mission (TRMM) sensor package, *J. Atmos. Oceanic Tech., 15,* 809-817, 1998.

Shin, D.-B., and G. R. North, Errors incurred in sampling a cyclostationary field, *J. Atmos. Oceanic Tech., 17,* 656-664, 2000.

Simpson, J., R. F. Adler and G. R. North, A proposed tropical rainfall measuring mission (TRMM), *Bull. Am. Meteorol. Soc., 69,* 278-295, 1988.

Simpson, J., Global circulation and tropical cloud activity, in *The Global Role of Tropical Rainfall,* edited by J. S. Theon, T. Matsuno, T. Sakata, and N. Fugono, pp. 77-92, A. Deepak Publishing, 1992.

Waliser, D. E., and C. Gautier, A satellite-derived climatology of the ITCZ, *J. Climate, 6,* 2162-2174, 1993.

Wilheit, T. T., A. T. C. Chang, and L. S. Chiu, Retrieval of monthly rainfall indices from microwave radiometric measurements using probability distribution functions, *J. Appl. Meteor., 16,* 551-560, 1991.

D.-B. Shin, L. S. Chiu and M. Kafatos, Center for Earth Observing and Space Research, School of Computational Sciences, George Mason University, Fairfax, VA 22030. (e-mail: dshin@science.gmu.edu)

(Received August 3, 2000; revised November 2, 2000; accepted November 10, 2000.)